Nonisothermal cellular automata simulation of two-dimensional snow crystal growth

X. Y. Xu and W. Wang*
Shanghai Jiao Tong University, 800 Dong Chuan Rd., Shanghai 200240, China

(Received 18 October 2021; revised 29 June 2022; accepted 21 September 2022; published 14 November 2022)

Natural snowflakes exhibit remarkable diversity with a fascinating sixfold symmetry and fractal structure. Efforts to discover the snow crystal growth pattern and mechanism behind it have been made in the past 50 years. Among those, cellular automata (CA) have made certain progress. To investigate the influence of latent heat release in snow crystal growth and have a deeper understanding of crystal growth characteristics, an improved CA model combined with vapor diffusion and heat diffusion is proposed to investigate the snowflake growth process in a two-dimensional and nonisothermal field in this paper. Simulation results show that obtained snow crystal growth behavior is consistent with previous experimental observations and satisfies the crystal growth dynamic theory. Latent heat release impacts the small structure of snow crystals, and it could have a more significant influence on snowflake morphology when vapor diffusion is slow and heat diffusion is dominating.

DOI: 10.1103/PhysRevE.106.055309

I. INTRODUCTION

Crystallization is a phase-change phenomenon existing widely in nature and industry. The fundamental phase transition during this process relates to thermodynamics, kinetics, and transport [1]. Snowflake (snow crystal) is one of the most common productions of natural crystallization. The exquisite construction of snowflakes depending on temperature and water-vapor humidity was first analyzed by Nakaya [2] with the microscopic observation of both natural and artificial snowflakes. Despite a rather clear picture of snowflake morphology, the growth mechanism behind it still needs deeper research [3,4]. Identifying and characterizing the growth process of ice crystals and simulating them with suitable mathematical models has been an ongoing process [5,6].

Attempts at snow crystal simulation have been done over the past 50 years. Among numerous models, cellular automata (CA) is one family of computational models which has been widely used in traffic simulation [7,8], network topological analysis [9], epidemic modeling [10], fluid dynamics study [11], and other fields [12,13]. Mackay [14] first suggested that CA could be used to simulate snowflake growth. Witten and Sander [15] introduced a groundbreaking prototype for dendritic crystal growth known as diffusion-limited aggregation (DLA). Packard [16] proposed an innovative variant of DLA and identified a CA model based on a triangular lattice with the evolution rule that a site having exactly one frozen neighbor always becomes frozen at the next update. Packard's cellular automata model inspired many researchers to develop it for better performance [17]. Coxe and Reiter [18,19] implemented fuzzy automata on a hexagonal array using simple arithmetic combinations of nearby fuzzy values and verified the possibility of fuzzy automata to maintain the symmetry of snowflakes and meanwhile exhibit great diversity depending on the background where they grew. Oz *et al.* [20] applied the cellular automaton lattice gas model to simulate and examine the formation and growth of snowflakes. Gravner and Griffeath [21,22] proposed their algorithm for snow crystal growth that combines DLA with anisotropic attachment kinetics and an idealized quasiliquid layer. Libbrecht [23] investigated the mechanism of crystal growth with the help of CA modeling and made a more systematical organization about assumptions of crystal growth with features like diffusion-limited growth, surface attachment kinetics, and structure-dependent attachment kinetics [24]. Kelly *et al.* [25] tried to connect physical variables with previous models and made a systematic survey of the morphologies resulting from their improved CA model. Li and Schaposnik [26] summerized Reiter's model and proposed a new geometric rule to incorporate interface control after analyzing the growth of snowflake images generated by Reiter's model. More recently, Liu *et al.* [27] simulated the process of snowflake formation from a pure water system with CA and studied the effects of model parameters on the crystal morphology. Besides, other numerical models for snowflake growth, like front-tracking [28] and phase-field methods [29], were developed in the meantime.

An isothermal hypothesis has always been given in former research ignoring temperature change during the snowflake growth process. Nevertheless, both temperature and humidity are important factors affecting the growth of snowflakes. Therefore, an improved cellular automata model with physically derived rules is proposed to study the two-dimensional snow crystal growth process in a nonisothermal field in this paper. Results are compared with experimental observations to give some explanations of snowflake growth characteristics, and parameters in this model are discussed to have a more profound understanding of crystal growth dynamics.

II. SYSTEM DESCRIPTION OF THE ICE CRYSTAL GROWTH FROM WATER VAPOR

Consider a domain $\Omega \in \mathbb{R}^2$ and the time interval $\Upsilon = (0, T)$ in which snow crystal grows from a small germ with

*wenwang@sjtu.edu.cn

initial water-vapor number density $c|_{t=0} = c_{\text{ini}}$ and initial temperature $\theta|_{t=0} = \theta^* - \Delta\theta_{\text{ini}}$, in which $\theta^* \approx 0\,^\circ\text{C}$ is the freezing-point temperature of water and $\Delta\theta_{\text{ini}}$ the initial subcooled degree. At each time t, $\Omega(t)$ can be divided into the solid-phase subdomain $\Omega_s(t)$, the gas-phase subdomain $\Omega_g(t)$, and the phase interface $\Gamma(t) = \Omega(t) - [\Omega_s(t) + \Omega_g(t)]$.

The diffusion equation in the gas phase is

$$\frac{\partial \sigma}{\partial \dot{t}} = \dot{D}\nabla^2\sigma, \tag{1}$$

where $\sigma = (c - c_{\text{sat}})/c_{\text{sat}}$ is the nondimensionalized concentration (supersaturation), c is the volumetric number density of water vapor, c_{sat} is the saturated vapor density, $\dot{D} = D\frac{t_0}{x_0^2}$ is the dimensionless vapor-diffusion coefficient, D is the vapor-diffusion constant in air, $\dot{t} = t/t_0$ is the dimensionless time, t_0 is the user-defined timescale, and x_0 is the user-defined length scale.

The growth velocity normal to the snow crystal surface in terms of the Hertz-Knudsen formula is written as [30]

$$v_\Gamma = \alpha\frac{c_{\text{sat}}}{c_s}\sqrt{\frac{k\theta_{\text{surf}}}{2\pi m}}\sigma_{\text{surf}}, \tag{2}$$

in which α is the attachment coefficient in the range of $10^{-6} \sim 1$, embodying the surface physics that governs how water molecules are incorporated into the ice lattice, collectively known as the attachment kinetics [6]. Besides, θ_{surf} is the temperature on the crystal surface, k is the Boltzmann constant, m is molar mass, and $c_s = (\rho_s \text{NA})/m$ is the crystal molecular number density and σ_{surf} is the supersaturation just above the growing surface.

The equation of continuity at $\Gamma(t)$ gives

$$\frac{\partial \sigma}{\partial \vec{n}} = v_\Gamma. \tag{3}$$

The heat transfer equation in $\Upsilon \times \Omega$ is

$$\frac{\partial \dot{\theta}}{\partial \dot{t}} = \dot{\lambda}\nabla^2\dot{\theta} + \dot{L}\frac{\partial \dot{m}_\Gamma}{\partial \dot{t}}, \tag{4}$$

in which $\dot{\theta} = (\theta - \theta^*)/\Delta\theta_{\text{ini}} + 1$ is the dimensionless temperature, $\dot{\lambda} = \frac{\lambda}{\rho c_p}\frac{t_0}{x_0^2}$ is the dimensionless heat-diffusion coefficient, λ is the thermal conductivity, ρ is the density, c_p is the specific heat capacity, $\dot{L} = L/(\rho c_p \Delta\theta_{\text{ini}})$ is the dimensionless latent heat of solidification, L is the latent heat,$\dot{m}_\Gamma = m_\Gamma/(V_\Gamma\rho_s)$ is the dimensionless crystal mass in the phase interface, V_Γ is the volume of interface, and ρ_s is the density of crystal.

Boundary conditions on $\Upsilon \times \partial\Omega$ are defined as

$$\begin{aligned} \sigma_{\partial\Omega} &= \sigma_{\text{ini}} \\ \dot{\theta}_{\partial\Omega} &= 0 \end{aligned} \tag{5}$$

The initial crystal germ deciding the initial solid and vapor phase domain is defined as

$$\Omega_s(0) = \Omega_{s,\text{ini}}. \tag{6}$$

III. SIMULATION MODEL

A combined method of the finite difference and the cellular automata is adopted in the proposed simulation model. With consideration of anisotropy in six directions of ice crystal, the computational domain Ω is divided by hexagonal grids with equal lattice spacing x_0 as shown in Fig. 1. Each grid is an element in finite difference and also a cellular automata cell, which means that both finite difference and cellular automata run on the same hexagonal lattice with the same time step t_0. By Taylor expansion and vector transformation, the discrete forms of Eq. (1) and Eq. (4) are obtained:

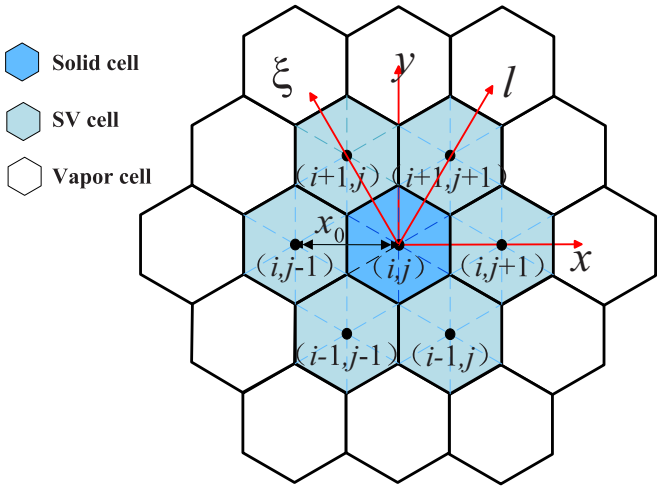

FIG. 1. Illustration of a node (i, j) with six adjacent nodes in a hexagonal lattice.

$$\begin{aligned} \sigma_{i,j}(t + t_0) = \frac{2\dot{D}}{3}[&\sigma_{i,j-1}(t) + \sigma_{i,j+1}(t) + \sigma_{i-1,j}(t) + \sigma_{i+1,j}(t) \\ &+ \sigma_{i-1,j-1}(t) + \sigma_{i+1,j+1}(t)] + (1 - 4\dot{D})\sigma_{i,j}(t), \end{aligned} \tag{7}$$

$$\begin{aligned} \dot{\theta}_{i,j}(t + t_0) = \frac{2\dot{\lambda}}{3}[&\dot{\theta}_{i,j-1}(t) + \dot{\theta}_{i,j+1}(t) + \dot{\theta}_{i-1,j}(t) + \dot{\theta}_{i+1,j}(t) \\ &+ \dot{\theta}_{i-1,j-1}(t) + \dot{\theta}_{i+1,j+1}(t)] + (1 - 4\dot{\lambda})\sigma_{i,j}(t) \\ &+ \dot{L}\Delta\dot{m}_\Gamma, \end{aligned} \tag{8}$$

where $\Delta\dot{m}_\Gamma$ is a quantity related to the crystal interface propagation and stands for the solidification mass which causes the release of latent heat. In other words, $\Delta\dot{m}_\Gamma$ is related to v_Γ. According to Eq. (2), attachment kinetics, which is parametrized by α, plays a nontrivial role in v_Γ. A definition of $\alpha = 1$ is given if water molecules striking the surface are instantly incorporated into it. For the faceted surface growth, it has $\alpha < 1$ [31]. More research about this is in Ref. [24]. In addition, the equilibrium vapor pressure on the crystal surface depends on surface curvature due to the Gibbs-Thomson effect [32], which is also important for snow crystal growth [33]. Therefore, the solution of Eq. (2) could be complex. To solve this, the cellular automata model is adopted and an improved algorithm is proposed based on Gravner and Griffeath's algorithm [21].

Each cell has three possible states corresponding to the solid, the vapor, and the solid-vapor (SV) interface as shown in Fig. 1. The six nearest cells around each cell are called the neighborhood. The dynamic state of each cell is decided by states of its neighborhood and also itself. Two different types of mass in cellular automata cells are defined: solid-crystal

mass contained in solid cells and water-vapor mass contained in vapor cells. Both solid-crystal mass and water-vapor mass exist in SV interface cells. The growth of snowflake is represented by the migration of the SV interface and it is divided into three steps:

(1) A portion of vapor mass in the SV interface cell turns into solid mass and the solidification proportion κ is defined as

$$\kappa = \varphi\sigma\sqrt{\theta}, \tag{9}$$

where φ is the solidification coefficient.

(2) The SV interface cell incorporates into the crystal (i.e., it turns into a solid cell) if its neighbors and itself satisfy the following criteria:

$$\begin{aligned} &\text{when N} = 1 \text{ or } 2, \text{ if } \dot{m}_\Gamma > \beta, \ \alpha = 1; \\ &\text{when } N = 3 \text{ or } 4, \text{ if either } \dot{m}_\Gamma > 1 \text{ or} \\ &\quad \sum_{\text{neighbor}} m_v > \psi \text{ and } m_\Gamma > \zeta, \ \alpha = 1; \\ &\text{when } N \geqslant 5, \ \alpha = 1; \end{aligned} \tag{10}$$

in which N is the neighboring crystal cells number of the calculated cell and $\sum_{\text{neighbor}} m_v$ is the vapor-mass sum of the neighborhood cells. In this incorporation process, the crystal mass in the SV interface cell has to reach a threshold value or the condition of the interface cell satisfies specific requirements; then, this interface cell immediately turns into a solid cell (which means $\alpha = 1$). When $N = 1$ or 2, the local mesoscopic geometry corresponds to a tip or flat spot of the crystal, where $\dot{m}_\Gamma$ has to reach a high value for a cell evolution (i.e., β is usually higher than 1). When $N = 3$ or 4, the threshold value is set as 1. Specific condition parametrized by ψ and ζ represents the knife-edge instability [34], which is a phenomenon that crystal plate could fill concavities even though the edges are very thin. Once the cell is sufficiently near the crystal, the attachment threshold becomes 0 ($N \geqslant 5$), precluding the formation of occasional single-cell holes in the snowflake [21].

(3) After the migration of the SV interface, the temperature would arise in the vicinity; some water molecules might return from the solid state into the water-vapor state if the temperature approaches θ^*, known as surface premelting [35]. It may affect the growth rates and shapes of snowflakes [36]. Define ϕ as the premelting proportion of crystal mass and it is decided by

$$\phi = \varepsilon\sigma\sqrt{\theta}, \tag{11}$$

where ε is the premelting coefficient. The treatment of κ and ϕ is inspired by Eq. (2).

IV. NUMERICAL RESULTS AND DISCUSSION

Simulations were performed using the hexagonal grid with spacing $x_0 = 0.0001$ m and time step $t_0 = 0.0001$ s, on a 500×500 simulation box with $\dot{D}$ defined as 3/14. The growth of snow crystals was initiated with a circular disk germ with homogeneous supersaturation σ_{ini} and uniform temperature $\theta = \theta^* - \Delta\theta_{\text{ini}}$. The initial disk germ radius was set as $3x_0$. The calculation procedures were programmed in MATLAB. Values of physical parameters are listed in Table I.

TABLE I. Values of physical parameters.

Parameter	SI units	Value
θ^*	K	273.15
ρ	kg m^{-3}	1.32 for dry air 917.00 for ice crystal
c_p	J kg^{-1} K^{-1}	1005.00 for air 2088.00 for ice crystal
λ	W m^{-1} K^{-1}	0.02 for air 2.01 for ice crystal
L	J m^{-3}	3.696×10^6
D	m^2 s^{-1}	2.00×10^{-5} [6]

A. Isothermal dendrite growth

The characteristics of dendrite crystal growth were first analyzed with an isothermal model by ignoring the heat-transfer equation. An isothermal growth case is shown in Fig. 2 and the initial supersaturation $\sigma_{\text{ini}} = 0.58$. During the crystal growth process, highly anisotropic surface tension and branching instability compete with each other. The anisotropic surface tension aims to minimize the crystal interfacial energy, which is responsible for the hexagonal symmetry and faceted aspect of snowflakes [1]. The branching instability is one of those instabilities to solidify the vapor, also called Mullins-Sekerka instability [37]. The surface structure of simulated dendrite crystal shows the same locus of competition between surface

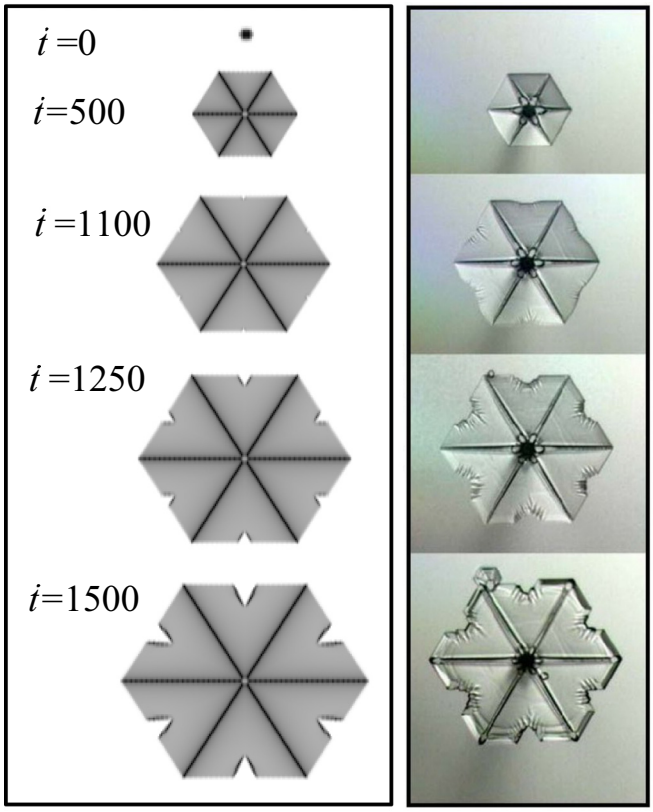

FIG. 2. Morphological comparison of snow crystal growth process between simulation results and experimental observation. Left: simulated results; Right: photos taken by Libbrecht [6].

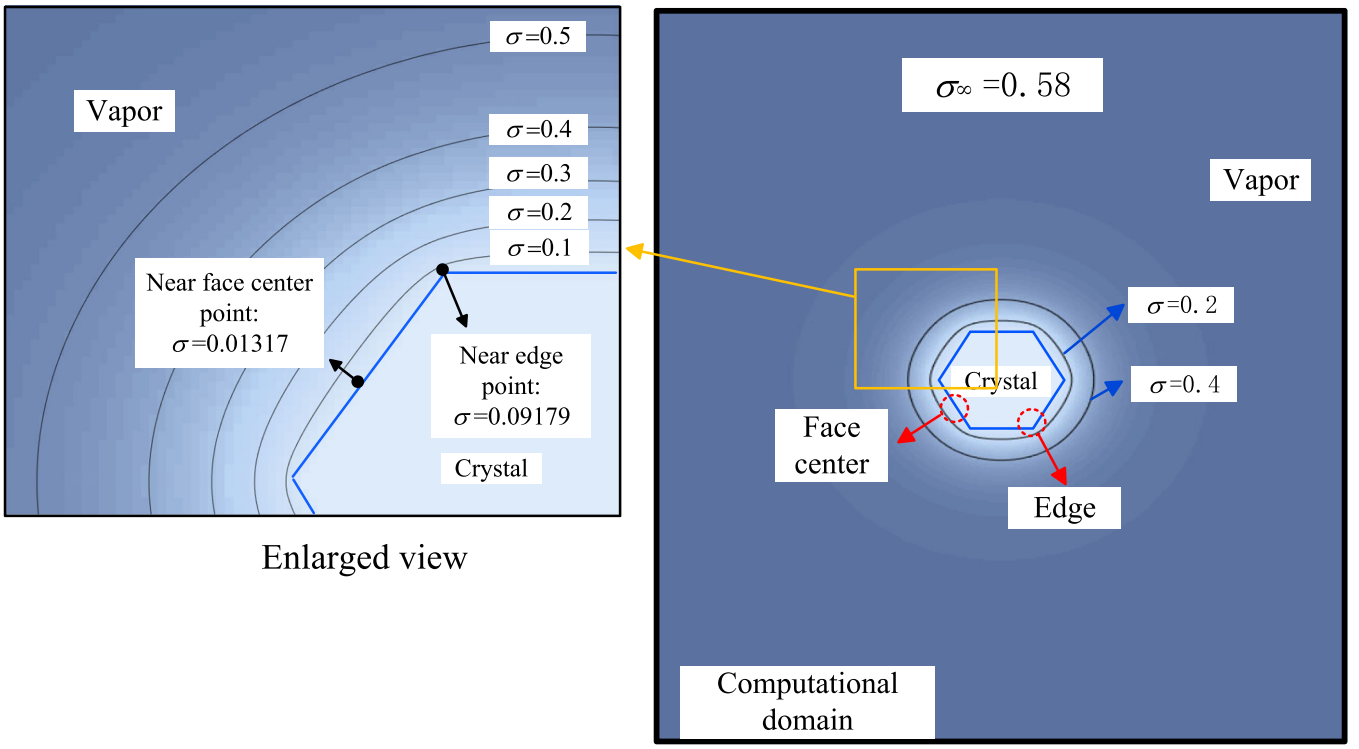

FIG. 3. Contour plot of supersaturation around the simulated crystal ($\dot{t} = 1000$).

tension and growth instability during crystal growth as the experimental observation when the simulated snow crystal growth process and the experimental snow crystal growth process are compared in Fig. 2. A quantitative comparison of size and time between simulation and experiment during the growth process is difficult due to the lack of sufficient experimental data. Following discussions about numerical results would be focused on the tendency and the regularity of growth characteristics based on the dimensionless time $\dot{t}$ and the dimensionless length $\dot{x}$.

In the initial stage, this snow crystal in Fig. 2 displays sharp edges that accord with the Wulff shape (the equilibrium shape of a crystal) [38] when $\dot{t} = 500$. Gradually, the divergence occurs at face centers resulting in six main branches. This branching instability relates to the Berg effect [39], setting forth the regular supersaturation field around a crystal. The supersaturation field around the crystal before six main branches appear is illustrated in Fig. 3. Contour lines of supersaturation are smooth while crystal edges are sharp, leaving the higher supersaturation at edges (e.g., one point near crystal edge has $\sigma = 0.091\,79$) and lower supersaturation at face centers (e.g., one point near face center has $\sigma = 0.013\,17$) as shown in the enlarged view. This difference in supersaturation eventually results in an increasing growth rate in the vicinity of edges. Once the surface tension anisotropy cannot offset this divergence, the facet breaks and the main branches appear.

B. Nonisothermal dendrite growth

With the proposed model, numerical results of a simulated crystal growth process in a nonisothermal field are shown in Fig. 4. One-sixth of every snowflake at a selected time and its temperature distribution are put together for a better exhibition. The initial supersaturation $\sigma_{\text{ini}} = 0.4$ and the initial subcooled degree $\Delta\theta_{\text{ini}} = 10$ K. As it shows, the snowflake gradually forms six main branches, and side branches are generated on the main branches when $\dot{t} \geqslant 1600$. Side branching also comes from the competition between anisotropic surface tension and branching instability. The side-branching process of the simulated snow crystal is qualitatively similar to that side branch formation process of a dendritic ice crystal with faceted tips grown in the air of 1×10^5 Pa at $-15\,^{\circ}$C [40]. Temperature around the growing crystal rises due to the propagation of the surface; then, the heat dissipates into the ambient air and the crystal would be cooled down. However, the crystal growth continues and temperature would still rise in the vicinity of the dendrite crystal branch tips. The timescale for water-vapor diffusion in the vicinity of a crystal is $\tau_{\text{vapor\_diffusion}} \approx R_c^2/D$, where R_c is a characteristic crystal size [6]. Besides, heat-diffusion timescale is $\tau_{\text{temperature\_diffusion}} \approx \rho c_p L_c^2/\lambda$, where L_c is the characteristic length. They are to be compared with the growth timescale $\tau_{\text{growth}} \approx 2R_c/v_\Gamma$. The ratio of $\tau_{\text{vapor\_diffusion}}$ and τ_{growth} for typical snow crystal growth is usually less than 10^{-5} [6], and the ratio of $\tau_{\text{thermal\_diffusion}}$ and τ_{growth} is less than 10^{-4} for crystal while less than 1 for water vapor in the calculated case. Consequently, water-vapor diffusion and heat diffusion may adjust the supersaturation σ and the crystal temperature θ_s much faster than the crystal shape changes; however, the air temperature θ_g around the crystal may respond a little slower.

When side branches grow continuously, solid-vapor interactions in the vicinity of branches are drastically reduced. Therefore, the growth in the perpendicular direction of the main branches is restrained, which is called the slow-growth direction. On the contrary, the main-branch tip is close to high-supersaturation area resulting in a higher growth speed

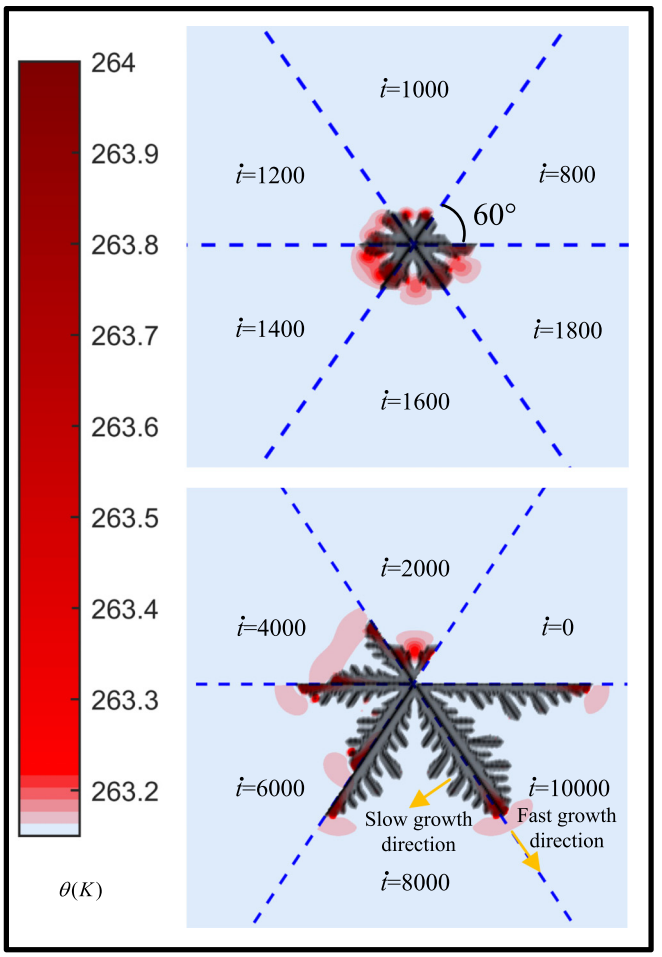

FIG. 4. Snow crystal growth and temperature field evolution.

and this direction is called the fast-growth direction. When $\dot{t} \leqslant 6000$, the growth in the slow-growth direction is still obvious; therefore, the heat release could be observed in this direction. After that, the main growth is in the fast-growth direction, and then side branches start to "shrink," leading to a keen-edged main branch ($\dot{t} = 10\,000$).

In Fig. 4, the temperature change is not significant and the temperature increment is less than 1 K during the growth process. The influence of temperature change due to the release of latent heat on snow morphology can be seen in Fig. 5, in which simulated snowflakes of an isothermal case and a nonisothermal case are compared. Their main branches have the same length and differ mainly in the morphology of side branches. For the isothermal case, the side branches at the end of the main branch are more uniform and nearly the same length, while for the nonisothermal case, side branches have unequal length distribution and the main-branch tip has a smaller edge angle. Therefore, the slight temperature disturbance changes the small structure of snowflakes.

As the fractal feature has been found in the simulated crystal and the snowflake dimensional properties have been studied using fractal geometry by former researchers [41], additional fractal analysis is applied to the growing crystal. The fractal dimension D_f is an indicator of how much space a mathematically described set occupies and it reflects the

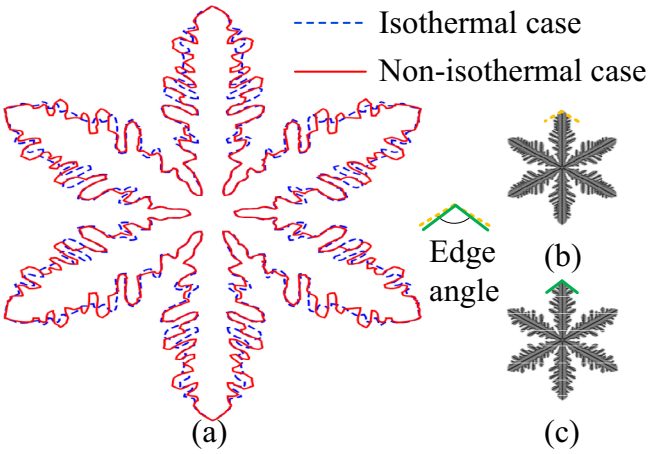

FIG. 5. Simulated snowflake comparison between an isothermal case and a nonisothermal case: (a) outline contrast, (b) the isothermal snowflake, and (c) the nonisothermal snowflake when $\dot{t} = 10\,000$.

validity of the occupied space of complex form [42]. For complex patterns like snowflakes, the box-counting method, which has been widely adopted for image analysis [43,44], is used to obtain D_f by a tool in MATLAB named Fraclab. Based on the box-counting algorithm, the relationship between D_f and snow crystal growth time of both the isothermal case and the nonisothermal case is depicted in Fig. 6.

Initial growths ($\dot{t} \leqslant 1950$) of the isothermal case and the nonisothermal case are the same. The initial value of D_f is close to 0 as it is an aggregation of several points set in a given manner and quickly increases to 1 if it grows a little bigger. The overall trend of D_f is on the increase while some decreasing points are found. The first decreasing point occurs at $\dot{t} = 550$ when the main branches start to appear. The rest of them are consistent with the occurrence of obvious side branches. Decreasing points of the nonisothermal growth are not the same as those of isothermal growth, especially when $\dot{t} \geqslant 6000$ as shown in the partially enlarged drawing. D_f of the nonisothermal case fluctuates more evidently and finally achieves a slightly higher value than that of the isothermal case. When the crystal grows to a certain size, the fluctu-

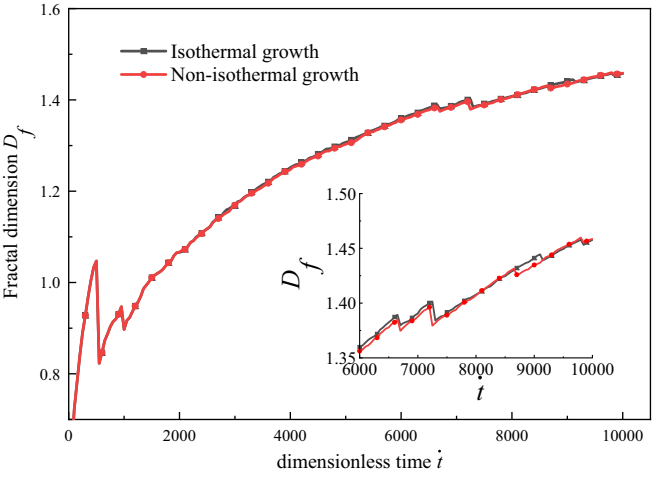

FIG. 6. Fractal dimension D_f of a growing crystal.

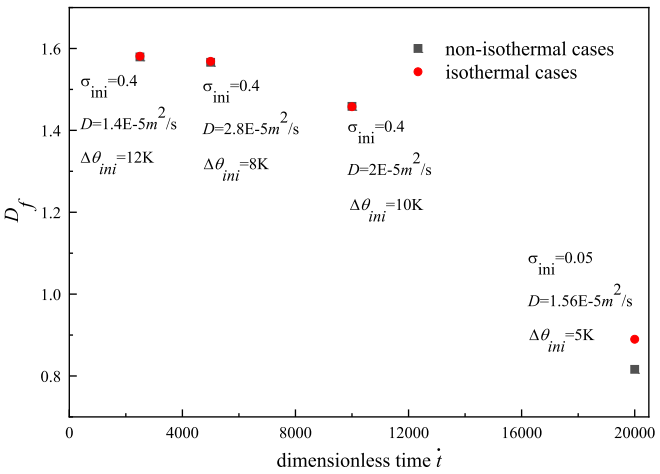

FIG. 7. Fractal dimension comparison between isothermal growth and nonisothermal growth with four different cases.

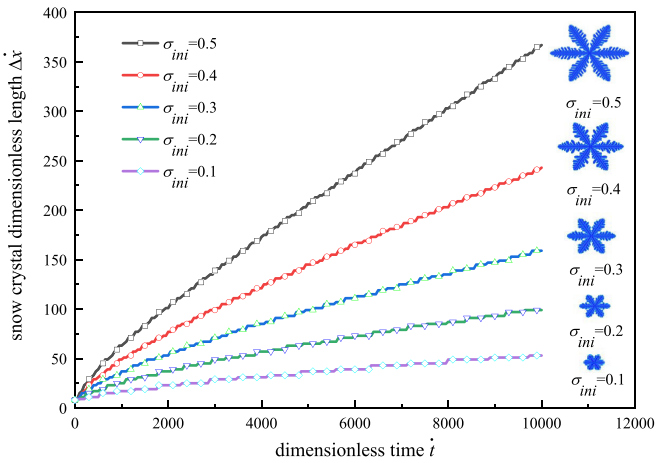

FIG. 8. Snow crystal length evolution when changing the initial supersaturation σ_{ini}.

ation range of D_f becomes smaller and D_f trends to be stable, meaning that increasing branches could not affect its complexity and the irregularity of the snowflake reaches a certain quantity. In summary, nonisothermal growth differs from isothermal growth in the late stage. When the growth environment has been changed, latent heat shows different degrees of impact on snowflake morphology if D_f of four different cases between isothermal growth and nonisothermal growth are compared in Fig. 7. D_f changes a little bit unless the initial supersaturation and initial subcooled degree are low ($\sigma_{\mathrm{ini}} = 0.05$, $\Delta\theta_{\mathrm{ini}} = 5$ K in Fig. 7). In this case, the crystal grows slowly and the final crystal size is very small when $\dot{t} = 20\,000$. Beyond that, the initial subcooled degree is low; therefore, temperature change due to latent heat release would be more significant. This indicates that latent heat release has a more pronounced effect on the morphology of snowflakes when heat diffusion plays a more dominating role.

C. Factors affecting snowflake growth

Both temperature and humidity are key factors influencing the snowflake morphology, and they are investigated, respectively, with this model. The variation of snow crystal length with time when changing the initial supersaturation σ_{ini} in the condition of the same initial subcooled degree $\Delta\theta_{\mathrm{ini}} = 10$ K is displayed in Fig. 8. Besides, the morphology of snowflakes when $\dot{t} = 10\,000$ with different σ_{ini} are also exhibited in Fig. 8.

Crystal length increases with increasing σ_{ini} and the slope of the crystal length curve standing for the crystal growth velocity of main-branch tips also increases as σ_{ini} increases. More side branches are generated if σ_{ini} increases. The higher the supersaturation is, the faster the edge grows, and then the crystal face center cannot form timely, leading to more splits in the face center. In the initial stage, branch tips grow fast and tip velocity decreases with time; then, it becomes a constant in the later growth process. Therefore, once the crystal grows in a relatively stable environment, the growth of the main branches would be stable as well. Usually, σ_{ini} in nature cannot reach so high as that in the simulation, but it still inspires the study of the snowflake growth pattern.

Variation of fractal dimension D_f with different σ_{ini} is also observed when the crystal goes through the same time $\dot{t} = 10\,000$ or the crystal reaches the same length ($\Delta\dot{x} = 53$) in Fig. 9. D_f is monotonically increasing as σ_{ini} increases because more side branches fill the space for the same growth time. The value of D_f changes a little as σ_{ini} increases when the crystal is at the same length. This indicates that increasing σ_{ini} speeds up the crystal growth but has little effect on the effectiveness of filling space.

Temperature influence on snow growth has also been analyzed by simulations with different initial subcooled degrees $\Delta\theta_{\mathrm{ini}}$ when σ_{ini} keeps a constant value of 0.4. The results are displayed in Fig. 10. First of all, the main branches of snow crystals become more slender and longer with more side branches, and the crystal length increases as well as $\Delta\theta_{\mathrm{ini}}$ increases. Apart from this, the envelope of the main-branch tips becomes sharper with a knifelike edge. It shows that when the subcooled degree increases, snow crystal speeds up in the fast-growth directions leading to gracile branches. The growth rate of main-branch tips observed by the slopes of curves in Fig. 10 shows a similar relationship as that in Fig. 8.

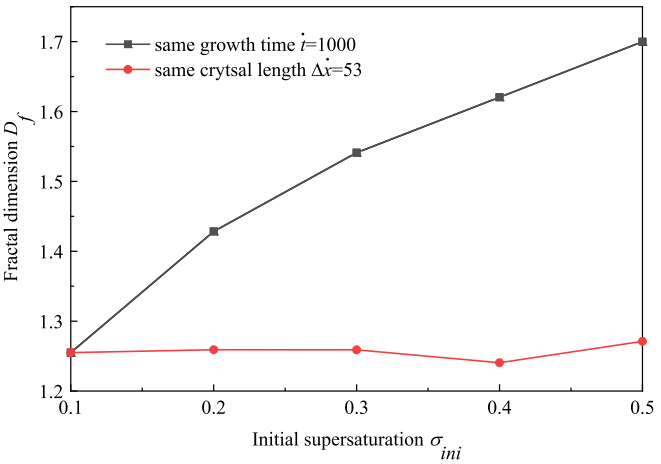

FIG. 9. Variation of fractal dimension D_f with different initial supersaturation σ_{ini}.

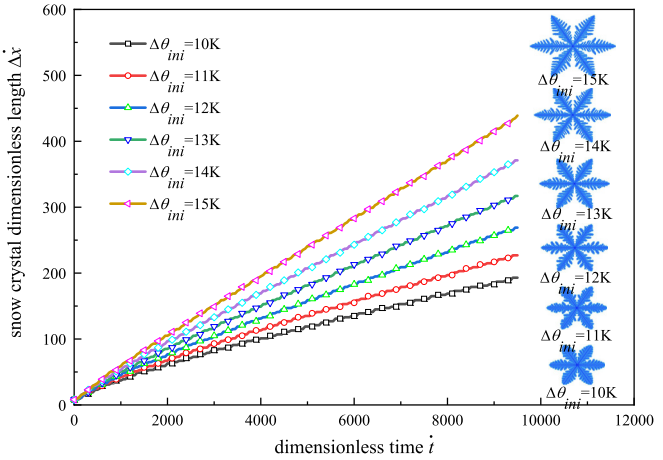

FIG. 10. Snow crystal length evolution when changing the initial subcooled degree $\Delta\theta_{\text{ini}}$.

Nevertheless, $\Delta\theta_{\text{ini}}$ has comparatively less effect on crystal interface normal velocity v_Γ than σ_{ini} does.

The relationship between fractal dimension D_f and the initial subcooled degree $\Delta\theta_{\text{ini}}$ is given in Fig. 11. When the crystals go through the same time ($\dot{t} = 9500$), D_f keeps rising if $\Delta\theta_{\text{ini}}$ increases while D_f has a little drop for $\Delta\theta_{\text{ini}} = 15$ K. On the contrary, D_f decreases with increasing $\Delta\theta_{\text{ini}}$ for the same crystal length. When $\Delta\theta_{\text{ini}}$ increases, the complexity and the irregularity of crystals reduce. Comparing the relationship between D_f and σ_{ini}, the temperature has less impact on crystal growth speed, but has a greater influence on the complexity of snow crystals than supersaturation does. The significant temperature change during growth could affect the entire structure of snowflakes.

V. CONCLUSIONS

In this work, an improved cellular automata model to simulate the snow crystal growth process in a nonisothermal field has been proposed. A system in which the snow crystal grew considering the interplay of vapor-mass diffusion, heat diffusion, and crystal growth kinetics was established. Simulation results are consistent with the experimental results.

During the crystal growth process, surface tension and growth instabilities play an important role in the generation of crystal main branches and side branches. Small temperature change due to latent heat release during the growth process impacts the small structure of snowflakes. Only when vapor diffusion is slow and heat diffusion becomes significant, latent heat release shows noticeable effects on snowflake morphology.

The effects of temperature and water-vapor concentration (represented by vapor supersaturation) have been investigated. Water-vapor concentration will accelerate the growth velocity and promote side branches. The temperature has a similar influence on crystal growth. Additional fractal analysis was employed to study snow crystal growth. According to the im-

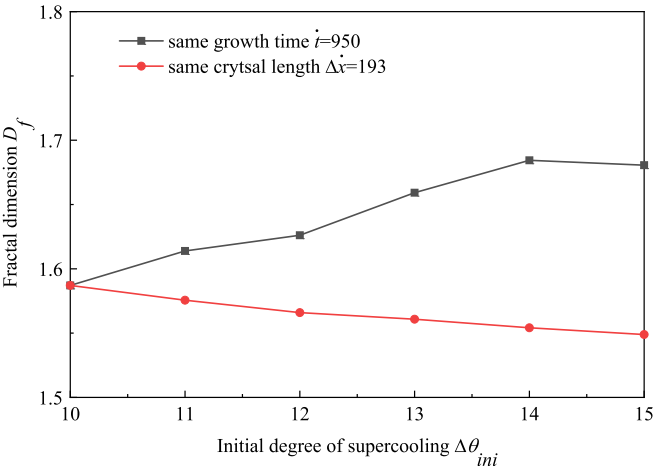

FIG. 11. Variation of fractal dimension D_f with a different initial subcooled degree $\Delta\theta_{\text{ini}}$.

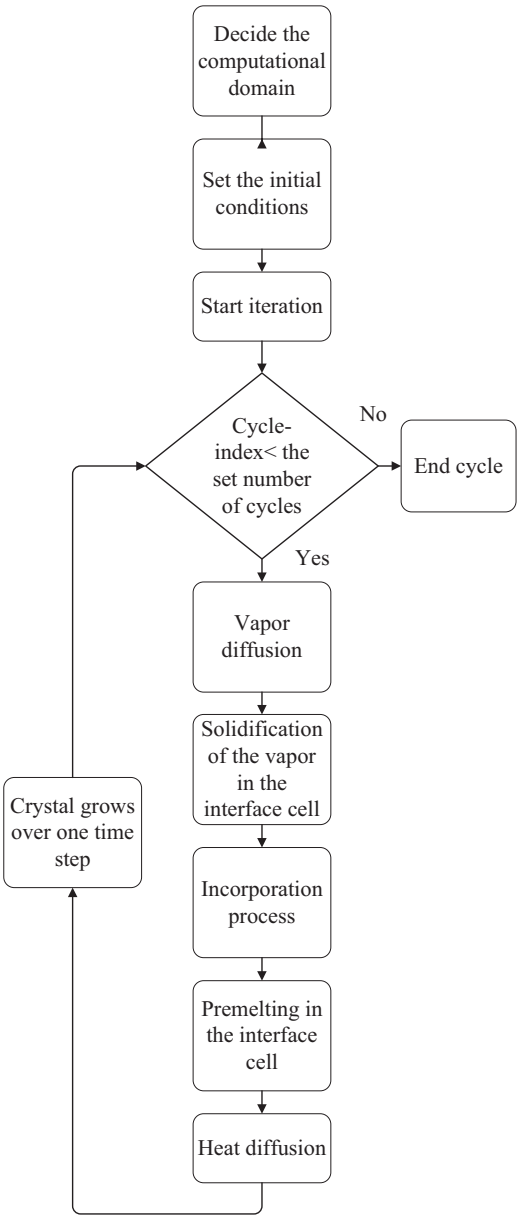

FIG. 12. Logical block diagram of the calculation procedures.

pact of temperature and water-vapor supersaturation on D_f, it can be concluded that temperature plays a more important role in the structural complexity of snowflakes than water-vapor supersaturation, while supersaturation affects crystal surface normal velocity more significantly than temperature does.

APPENDIX A: DISCRETIZATION OF GOVERNING EQUATIONS

The discrete form of vapor-mass diffusion Eq. (1) in this lattice can be derived through Taylor expansion and vector transformation. For a chosen node (i, j) with six adjacent nodes shown in Fig. 1, Taylor series expansions of its neighbors based on $\sigma_{i,j}(t)$ are

$$\sigma_{i+h,j+k}(t) = \sigma_{i,j}(t) + (hk)(\nabla\sigma \cdot \vec{e}_{i+h,j+k})x_0 + \frac{1}{2!}[\nabla \cdot (\nabla\sigma \cdot \vec{e}_{i+h,j+k})]x_0^2 + x_0^3(0), \quad \text{(A1)}$$

where $h = 0, 1,$ and -1; $k = 0, 1,$ and -1, and $h \neq k$. Besides, $\vec{e}_{i+h,j+k}$ is the unit vector from point $(i + h,\ j + k)$ to (i, j), which can also be expressed by $\vec{l}$, $\vec{\xi}$, and $\vec{x}$ as Fig. 1 shows. The direction vector σ_l can be expressed by σ_x and σ_y through vector transformation:

$$\sigma_l = \sigma_x \cos 60^\circ + \sigma_y \cos 30^\circ = \frac{1}{2}\sigma_x + \frac{\sqrt{3}}{2}\sigma_y. \quad \text{(A2)}$$

Therefore, the second-order derivative σ_{ll} is

$$\begin{aligned}\sigma_{ll} &= \frac{\partial}{\partial x}\left[\frac{1}{2}\sigma_x + \frac{\sqrt{3}}{2}\sigma_y\right]\cos 60^\circ \\ &\quad + \frac{\partial}{\partial y}\left[\frac{1}{2}\sigma_x + \frac{\sqrt{3}}{2}\sigma_y\right]\cos 30^\circ \\ &= \frac{1}{4}\sigma_{xx} + \frac{\sqrt{3}}{2}\sigma_{xy} + \frac{3}{4}\sigma_{yy}. \end{aligned} \quad \text{(A3)}$$

Similarly, $\sigma_{\xi\xi}$ can be expressed as

$$\sigma_{\xi\xi} = \frac{1}{4}\sigma_{xx} - \frac{\sqrt{3}}{2}\sigma_{xy} + \frac{3}{4}\sigma_{xy}. \quad \text{(A4)}$$

Besides, Taylor expansion of $\sigma_{i,j}(t + t_0)$ based on $\sigma_{i,j}(t)$ is

$$\sigma_{i,j}(t + t_0) = \sigma_{i,j}(t) + \sigma_t t_0 + t_0^2(0). \quad \text{(A5)}$$

By adding Eq. (1) together and then substituting Eqs. (3)–(5) in it, the discrete form of $\sigma_{i,j}(t + t_0)$ ignoring the second-order small term is obtained as

$$\begin{aligned}&\sigma_{i,j}(t + t_0) \\ &= \frac{2\dot{D}}{3}[\sigma_{i,j-1}(t) + \sigma_{i,j+1}(t) + \sigma_{i-1,j}(t) + \sigma_{i+1,j}(t) \\ &\quad + \sigma_{i-1,j-1}(t) + \sigma_{i+1,j+1}(t)] + (1 - 4\dot{D})\sigma_{i,j}(t). \end{aligned} \quad \text{(A6)}$$

The similar discrete equation for heat transfer is given as

$$\begin{aligned}\dot{\theta}_{i,j}(t + t_0) = \frac{2\dot{\lambda}}{3}&[\dot{\theta}_{i,j-1}(t) + \dot{\theta}_{i,j+1}(t) + \dot{\theta}_{i-1,j}(t) \\ &+ \dot{\theta}_{i+1,j}(t) + \dot{\theta}_{i-1,j-1}(t) + \dot{\theta}_{i+1,j+1}(t)] \\ &+ (1 - 4\dot{\lambda})\sigma_{i,j}(t) + \dot{L}\Delta\dot{m}_\Gamma. \end{aligned} \quad \text{(A7)}$$

APPENDIX B: CALCULATION PROCEDURE

The logical block diagram of our procedure is shown in Fig. 12. The program is combined with a main program and several subprograms. After deciding the computational domain and setting the initial conditions, the main program enters the loop. Each loop stands for a growth period in a time step. During this period, the vapor supersaturation field is first calculated through the discretized vapor-diffusion equation in the gas zone. Then, three steps in the cellular automata model proceed in sequence and the SV interface would migrate, indicating crystal growth. After that, the solidification mass $\Delta\dot{m}_\Gamma$ in the interface can be calculated and the temperature field would be calculated through the discretized heat-diffusion equation. The state in every cell would be defined and this cycle is finished. By repeating this procedure, the crystal growth is simulated.

[1] J. C. Brice and P. Rudolph, Prog. Cryst. Growth Charact. **4**, iii (1981).
[2] U. Nakaya, in *Snow Crystals* (Harvard University Press, Cambridge, 2013).
[3] R. Lacmann and I. N. Stranski, J. Cryst. Growth **236** 13 (1972).
[4] J. Nelson, Philos. Mag. A **81**, 2337 (2001).
[5] K. G. Libbrecht, Eng. Sci. **64**, 10 (2001).
[6] K. G. Libbrecht, Rep. Prog. Phys. **68**, 855 (2005).
[7] N. Moussa, Phys. Rev. E **68**, 036127 (2003).
[8] R. Jiang, Q.-S. Wu, and B.-H. Wang, Phys. Rev. E **66**, 036104 (2002).
[9] M. Šuvakov and B. Tadić, in *International Conference on Computational Science* (Springer, Berlin, Heidelberg, 2006), pp. 1098.
[10] Q.-X. Liu, Z. Jin, and M.-X. Liu, Phys. Rev. E **74**, 031110 (2006).
[11] R. Azevedo, R. Montenegro-Filho, and M. J. P. R. E. Coutinho-Filho, Phys. Rev. E **88**, 033022 (2013).
[12] M. Bernaschi, S. Succi, and F. Castiglione, Phys. Rev. E **61**, 1851 (2000).
[13] F. G. Pazzona, P. Demontis, and G. B. Suffritti, Phys. Rev. E **90**, 023307 (2014).
[14] A. Mackay, Phys. Bull. **27**, 495 (1976).
[15] T. A. Witten and L. M. Sander, Phys. Rev. Lett. **47**, 1400 (1981).
[16] N. H. Packard, in *Proceedings of 1st International Symposium for Science on Form* (Sakura, Japan, 1985), pp. 95.
[17] T. C. Halsey, Phys. Today **53** (11), 36 (2000).
[18] A. M. Coxe and C. A. Reiter, Vector **19**, 113 (2003).
[19] A. M. Coxe and C. A. Reiter, Comput. Graphics **27**, 447 (2003).
[20] S. Oz and B. Kutlu, in *the 9th WMO Weather Modification Conference* (ResearchGate, Antalya,Turkey, 2007), p. 1.
[21] J. Gravner and D. Griffeath, Phys. Rev. E **79**, 011601 (2009).

[22] J. Gravner and D. Griffeath, Physica D **237**, 385 (2008).
[23] K. G. Libbrecht, J. Comput. Methods Phys. **2013**, 174806 (2013).
[24] K. G. Libbrecht, J. Cryst. Growth **258**, 168 (2003).
[25] J. Kelly and E. Boyer, Cryst. Growth Des. **14**, 1392 (2014).
[26] J. C. Li and L. P. Schaposnik, Physical Rev. E **93**, 023302 (2016).
[27] J. Liu, J. Dai, C. Han, J. Zhang, J. Ai, C. Zhai, X. Liu, and W. Sun, in *Computer Aided Chemical Engineering* (Elsevier, Milano, Italy, 2020), Vol. 48, pp. 187.
[28] R. Kobayashi, Physica D **63**, 410 (1993).
[29] G. Demange, R. Patte, H. Zapolsky, and M. Brunel, npj Comput. Mater. **3**, 15 (2017).
[30] K. G. Libbrecht, Annu. Rev. Mater. Res. **47**, 271 (2017).
[31] Y. Saito, *Statistical Physics of Crystal Growth* (World Scientific, Singapore, 1996).
[32] M. Perez, Scr. Mater. **52**, 709 (2005).
[33] F. Almgren and L. Wang, J. Geom. Anal. **10**, 1 (2000).
[34] K. G. Libbrecht, Am. Sci. **95**, 52 (2007).
[35] J. S. Wettlaufer and M. G. Worster, Annu. Rev. Fluid Mech. **38**, 427 (2006).
[36] J. G. Dash, A. W. Rempel, and J. S. Wettlaufer, Rev. Mod. Phys. **78**, 695 (2006).
[37] W. Mullins and R. Sekerka, J. Appl. Phys. **34**, 323 (1963).
[38] L. Wang, F. Zhou, Y. S. Meng, and G. Ceder, Phys. Rev. B **76**, 165435 (2007).
[39] W. Berg, Proc. R. Soc. London, Ser. A: Math. Phys. Sci. **164**, 79 (1938).
[40] T. Gonda and S. Nakahara, J. Cryst. Growth **173**, 189 (1997).
[41] C. G. Schmitt and A. J. Heymsfield, J. Atmos. Sci. **67**, 1605 (2010).
[42] K. Falconer and Kenneth, *Fractal Geometry: Mathematical Foundations and Applications*, 2nd edition (John Wiley & Sons Ltd, England, 2003), p. 329.
[43] N. Sarkar and B. Chaudhuri, IEEE Trans. Syst., Man, Cybern., **24**, 115 (1994).
[44] J. Jiménez and J. Ruiz de Miras, Comput. Methods Programs Biomed. **108**, 1229 (2012).